The Static Magnetic Field Dependence of Chemical Exchange Linebroadening Defines the NMR Chemical Shift Time Scale

Oscar Millet,[†] J. Patrick Loria,[‡] Christopher D. Kroenke,[‡] Miquel Pons,[†] and Arthur G. Palmer, III*[,‡]

Contribution from the Departament de Química Orgànica, Universitat de Barcelona, Martí i Franquès 1-11, E-08028 Barcelona, Spain, and Department of Biochemistry and Molecular Biophysics, Columbia University, 630 West 168th Street, New York, New York 10032

Received September 29, 1999. Revised Manuscript Received January 7, 2000

Abstract: The static magnetic field dependence of chemical exchange linebroadening in NMR spectroscopy is investigated theoretically and experimentally. Two-site exchange ($A \leftrightarrows B$) is considered with site A more highly populated than site B ($p_a > p_b$), a shift difference between sites equal to $\Delta\omega$, and an exchange rate constant given by k_{ex}. The exchange contribution to the transverse relaxation rate constant for the more highly populated site is denoted R_{ex}. The dependence of R_{ex} on the static magnetic field strength is characterized by a scaling parameter $\alpha = d \ln R_{ex}/d \ln \Delta\omega$, in which $0 \leq \alpha \leq 2$ for $p_a > 0.7$. The value of α depends on the NMR chemical shift time scale for the exchange process: for slow exchange ($k_{ex}/\Delta\omega < 1$), $0 \leq \alpha < 1$; for intermediate exchange ($k_{ex}/\Delta\omega = 1$), $\alpha = 1$; and for fast exchange ($k_{ex}/\Delta\omega > 1$), $1 < \alpha \leq 2$. Consequently, the static magnetic field dependence of R_{ex} defines the chemical shift time scale for an exchange process even if the populations are so highly skewed ($p_a \gg p_b$) that the minor resonance is not observable in the slow exchange limit. The theoretical results are verified by measuring ^{15}N transverse relaxation rate constants at static magnetic fields of 11.7 and 14.1 T and temperatures of 300 and 313 K for the protein basic pancreatic trypsin inhibitor. At each combination of static magnetic field and temperature, the rate constants were measured using Carr−Purcell−Meiboom−Gill and Hahn echo techniques with spin−echo delays ranging from 1.0 to 64.5 ms. ^{15}N resonances for residues in the region of the Cys14-Cys38 disulfide bond are broadened due to chemical exchange. Values of α obtained from the relaxation rate constants range from 0.26 ± 0.17 for Arg39 at 300 K to 1.96 ± 0.25 for Cys38 at 313 K. For Cys38 and Arg39, the two residues most strongly affected by chemical exchange, values of k_{ex} were determined to be 380 ± 70 s^{-1} and 530 ± 90 s^{-1} at 300 K and 1300 ± 290 s^{-1} and 1370 ± 160 s^{-1} at 313 K by global analysis of the relaxation rate constants. The scaling parameters α indicate that chemical exchange for most residues in basic pancreatic trypsin inhibitor does not satisfy $k_{ex}/\Delta\omega \gg 1$. Consequently, the assumption of fast-limit quadratic scaling of exchange broadening in proteins and other macromolecules may be incorrect, even if a single broadened resonance is observed for a nuclear spin. The theoretical results for the static magnetic field dependence of chemical exchange broadening in NMR spectroscopy are applicable to other nuclei and to other techniques for measuring chemical exchange linebroadening.

Introduction

Knowledge of molecular dynamics is essential for understanding the biophysical properties and biological functions of proteins.[1,2] NMR spin relaxation measurements have proven to be a powerful tool for the characterization of dynamic processes in proteins in solution over a wide range of time scales.[3,4] Fast motions on picosecond−nanosecond time scales that modulate the chemical shift, dipolar coupling, and quadrupolar coupling can be characterized by heteronuclear (^2H, ^{13}C, and ^{15}N) spin relaxation NMR spectroscopy using established experimental protocols.[5] Recent applications of these techniques have focused on the role of conformational entropy in ligand binding[6,7] and protein folding.[8,9] Chemical or conformational kinetic processes on microsecond−millisecond time scales that stochastically transfer nuclear spins between magnetic environments with different isotropic chemical shifts, referred to generically as chemical exchange, also can be studied by NMR spectroscopy.[5] Chemical exchange contributes to the transverse relaxation rate in the laboratory frame (R_2) and in the rotating frame ($R_{1\rho}$). Consequently, chemical exchange can be characterized by measuring the excess contribution to the transverse relaxation rate constant, commonly called R_{ex}. Although experimental methods for characterizing motions on microsecond−milli-

* Author to whom correspondence should be addressed. Telephone: (212) 305-8675. Fax: (212) 305-7932). E-mail: agp6@columbia.edu.
† Universitat de Barcelona.
‡ Columbia University.

(1) Karplus, M.; McCammon, J. A. *Annu. Rev. Biochem.* **1983**, *53*, 263−300.
(2) Frauenfelder, H.; Sligar, S. G.; Wolynes, P. G. *Science* **1991**, *254*, 1598−1603.
(3) Palmer, A. G. *Curr. Opin. Struct. Biol.* **1997**, *7*, 732−737.
(4) Kay, L. E. *Nat. Struct. Biol.* **1998**, *5*, 513−517.
(5) Palmer, A. G.; Williams, J.; McDermott, A. *J. Phys. Chem.* **1996**, *100*, 13293−13310.
(6) Kay, L. E.; Muhandiram, D. R.; Wolf, G.; Shoelson, S. E.; Forman-Kay, J. D. *Nat. Struct. Biol.* **1998**, *5*, 156−163.
(7) Bracken, C.; Carr, P. A.; Cavanagh, J.; Palmer, A. G. *J. Mol. Biol.* **1999**, *285*, 2133−2146.
(8) Yang, D.; Kay, L. E. *J. Mol. Biol.* **1996**, *263*, 369−382.
(9) Alexandrescu, A. T.; Rathgeb-Szabo, K.; Rumpel, K.; Jahnke, W.; Schulthess, T.; Kammerer, R. A. *Protein Sci.* **1998**, *7*, 389−402.

10.1021/ja993511y CCC: $19.00 © 2000 American Chemical Society
Published on Web 03/14/2000

second time scales are not as well-established as the experimental methods for faster motions, a number of new techniques have been developed that are reinvigorating the investigation of chemical exchange in proteins.[10−15] Recent applications of these techniques include investigations of ligand binding,[16] loop and domain motions in enzymatic catalysis,[17] and protein conformational changes.[14,18]

For simplicity in the following, only the two-site exchange reaction is considered:

$$A \underset{k_{-1}}{\overset{k_1}{\rightleftharpoons}} B \tag{1}$$

in which the exchange rate constant, k_{ex}, is defined as[19]

$$k_{ex} = k_1 + k_{-1} = k_1/p_b = k_{-1}/p_a \tag{2}$$

p_a is the equilibrium population of site A, p_b is the equilibrium population of site B, $p_a + p_b = 1$, k_1 is the forward first-order kinetic rate constant, and k_{-1} is the reverse first-order kinetic rate constant. The two sites are assumed to have distinct chemical shifts ω_a and ω_b, respectively. The frequency difference between the chemical shifts of the two sites is $\Delta\omega = |\omega_a - \omega_b| = |\gamma\Delta\sigma B_0|$, in which γ is the gyromagnetic ratio for the exchanging nuclear spin, $\Delta\sigma$ is the difference in chemical shielding of the two sites, and B_0 is the static magnetic field strength. The transverse relaxation rate constants for sites A and B in the absence of conformational exchange are denoted R_a and R_b, respectively. The contribution to the line width or transverse relaxation rate constant from a chemical kinetic process depends critically on whether the exchange process is slow ($k_{ex}/\Delta\omega < 1$), intermediate ($k_{ex}/\Delta\omega \approx 1$), or fast ($k_{ex}/\Delta\omega > 1$) on the NMR chemical shift time scale.[20] If the populations of the two sites are similar, then slow exchange is recognized easily by the presence of two resolved resonances with frequencies ω_a and ω_b, while fast exchange is recognized by the presence of a single averaged resonance with frequency $p_a\omega_a + p_b\omega_b$. Unfortunately, as emphasized by Ishima and Torchia,[12] in many cases of interest, the populations of the sites are highly unequal. For example, if site A is more stable than site B by only $2k_BT$, in which k_B is the Boltzmann constant, then $p_a = 0.88$ and $p_b = 0.12$. In the slow exchange limit, the resonance at ω_b is both lower intensity, by a factor p_b/p_a, and significantly broader, by a factor $(R_b + p_ak_{ex})/(R_a + p_bk_{ex})$, than the resonance at ω_a. As a result, if $p_a \gg p_b$, then the resonance at ω_b may be undetectable. Thus, the mere observation of a single exchange-broadened resonance does not necessarily indicate that the exchange process is fast on the chemical shift time scale.

In the following, the dependence of the exchange contribution to the transverse relaxation rate constant on the static magnetic field strength is investigated. In contrast to statements in the literature that exchange broadening depends quadratically on the static magnetic field strength,[21−24] R_{ex} for the more highly populated site A is demonstrated to depend on the static magnetic field strength through the scaling relationship $\delta R_{ex}/R_{ex} = \alpha\ \delta B_0/B_0$, in which $0 \le \alpha \le 2$ for $p_a > 0.7$. The value of α depends on the NMR chemical shift time scale for the exchange process. Quadratic scaling of R_{ex} is obtained only for $\alpha \rightarrow 2$, and R_{ex} is independent of the static magnetic field for $\alpha \rightarrow 0$. Thus, the static magnetic field dependence of R_{ex} defines the chemical shift time scale for a chemical exchange process even if the populations are highly skewed with $p_a \gg p_b$. The theoretical results are verified using ^{15}N Carr−Purcell−Meiboom−Gill (CPMG)[25,26] measurements of transverse relaxation for basic pancreatic trypsin inhibitor (BPTI). A conformational exchange process in the region of the Cys14-Cys38 disulfide bond has been studied extensively by NMR spectroscopy.[14,27−29] Over the temperature range from 300 to 313 K, most of the exchange-broadened resonances in BPTI have values of α between 0.5 and 1.6; thus, exchange is neither very slow ($k_{ex}/\Delta\omega \ll 1$) nor very fast ($k_{ex}/\Delta\omega \gg 1$) on the chemical shift time scale. The results suggest that the assumption of fast-limit quadratic scaling of exchange broadening in proteins and other macromolecules generally is not tenable.

Theory

The contributions to transverse relaxation rate constants from chemical exchange processes in macromolecules most commonly are measured using CPMG[14,30] or $R_{1\rho}$ measurements.[10,11,28] The theoretical treatment of chemical exchange is more highly developed for the CPMG experiment[19,31] than for the $R_{1\rho}$ experiment.[32,33] In addition, the experimental results reported herein use the CPMG method to measure the effects of chemical exchange on ^{15}N transverse relaxation rate constants in BPTI. Accordingly, the theoretical presentation below focuses on the CPMG technique; however, similar conclusions regarding the static magnetic field dependence of conformational exchange are applicable to $R_{1\rho}$ measurements.

A general expression for the phenomenological transverse relaxation rate constant for site A, $R_2(1/\tau_{cp})$, is given by,[19,31]

$$R_2(1/\tau_{cp}) = {}^1/_2\left(R_a + R_b + k_{ex} - \frac{1}{\tau_{cp}}\cosh^{-1}[D_+\cosh(\eta_+) - D_-\cos(\eta_-)]\right) \tag{3}$$

in which τ_{cp} is the delay between 180° pulses in the CPMG

(10) Akke, M.; Palmer, A. G. *J. Am. Chem. Soc.* **1996**, *118*, 911−912.
(11) Zinn-Justin, S.; Berthault, P.; Guenneugues, M.; Desvaux, H. *J. Biomol. NMR* **1997**, *10*, 363−372.
(12) Ishima, R.; Wingfield, P. T.; Stahl, S. J.; Kaufman, J. D.; Torchia, D. A. *J. Am. Chem. Soc.* **1998**, *120*, 10534−10542.
(13) Konrat, R.; Tollinger, M. *J. Magn. Reson.* **1999**, *13*, 213−221.
(14) Loria, J. P.; Rance, M.; Palmer, A. G. *J. Am. Chem. Soc.* **1999**, *121*, 2331−2332.
(15) Mulder, F. A. A.; van Tilborg, P. J. A.; Kaptein, R.; Boelens, R. *J. Biomol. NMR* **1999**, *13*, 275−288.
(16) Evenäs, J.; Forsén, S.; Malmendal, A.; Akke, M. *J. Mol. Biol.* **1999**, *289*, 603−607.
(17) Ishima, R.; Freedberg, D.; Wang, Y.-X.; Louis, J. M.; Torchia, D. A. *Structure* **1999**, *7*, 1047−1055.
(18) Akke, M.; Liu, J.; Cavanagh, J.; Erickson, H. P.; Palmer, A. G. *Nat. Struct. Biol.* **1998**, *5*, 55−59.
(19) Davis, D. G.; Perlman, M. E.; London, R. E. *J. Magn. Reson., Ser. B* **1994**, *104*, 266−275.
(20) Cavanagh, J.; Fairbrother, W. J.; Palmer, A. G.; Skelton, N. J. *Protein NMR Spectroscopy: Principles and Practice*; Academic Press: San Diego, 1996; p 587.
(21) Farrow, N. A.; Zhang, O.; Szabo, A.; Torchia, D. A.; Kay, L. E. *J. Biomol. NMR* **1995**, *6*, 153−162.
(22) Mandel, A. M.; Akke, M.; Palmer, A. G. *J. Mol. Biol.* **1995**, *246*, 144−163.
(23) Peng, J.; Wagner, G. *Biochemistry* **1995**, *34*, 16733−16752.
(24) Phan, I. Q. H.; Boyd, J.; Campbell, I. D. *J. Biomol. NMR* **1996**, *8*, 369−378.
(25) Carr, H. Y.; Purcell, E. M. *Phys. Rev.* **1954**, *94*, 630−638.
(26) Meiboom, S.; Gill, D. *Rev. Sci. Instrum.* **1958**, *29*, 688−691.
(27) Otting, G.; Liepinsh, E.; Wüthrich, K. *Biochemistry* **1993**, *32*, 3571−3582.
(28) Szyperski, T.; Luginbühl, P.; Otting, G.; Güntert, P.; Wüthrich, K. *J. Biomol. NMR* **1993**, *3*, 151−164.
(29) Beeser, S. A.; Goldenberg, D. P.; Oas, T. G. *J. Mol. Biol.* **1997**, *269*, 154−164.
(30) Orekhov, V. Y.; Pervushin, K. V.; Arseniev, A. S. *Eur. J. Biochem.* **1994**, *219*, 887−896.

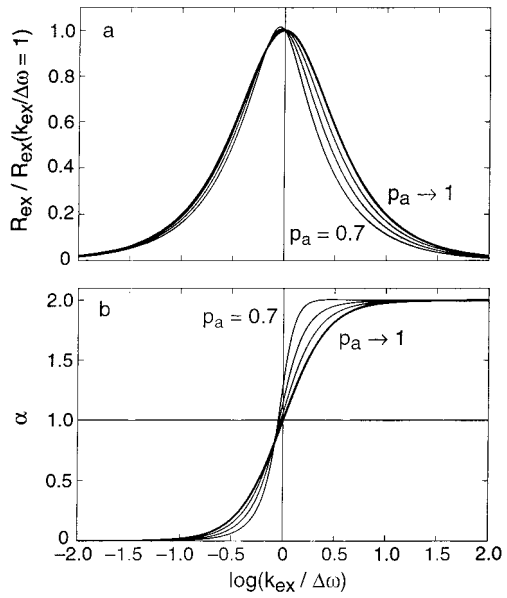

Figure 1. Chemical exchange and the NMR chemical shift time scale. The values of (a) R_{ex}, calculated from eq 8, and (b) α, calculated from eq 13, are shown as functions of k_{ex}. Values of R_{ex} are normalized by the value of R_{ex} at coalescence ($k_{ex}/\Delta\omega = 1$), and the *x*-axis is normalized by $\Delta\omega$ for presentation. The slow exchange regime corresponds to $k_{ex}/\Delta\omega < 1$, and the fast exchange regime corresponds to $k_{ex}/\Delta\omega > 1$. Curves are drawn for site populations $p_a \rightarrow 1$ (heavy line), 0.9, 0.8, and 0.7. Calculations were performed assuming $R_a = R_b$ and $\Delta\omega = 628\ s^{-1}$ (100 Hz), but the shapes of the resulting curves depend weakly on these assumptions. The results for α with $p_a \rightarrow 1$ are identical to eq 14.

pulse train,

$$D_{\pm} = {}^1/_2\left[\pm 1 + \frac{\psi + 2\Delta\omega^2}{(\psi^2 + \zeta^2)^{1/2}}\right] \tag{4}$$

$$\eta_{\pm} = \frac{\tau_{cp}}{\sqrt{2}}[\pm\psi + (\psi^2 + \zeta^2)^{1/2}]^{1/2} \tag{5}$$

$$\psi = (R_a - R_b - p_a k_{ex} + p_b k_{ex})^2 - \Delta\omega^2 + 4p_a p_b k_{ex}^2 \tag{6}$$

$$\zeta = 2\Delta\omega(R_a - R_b - p_a k_{ex} + p_b k_{ex}) \tag{7}$$

Evaluation of these equations for particular sets of parameters can depend on the proper choice of positive or negative square roots in eqs 4 and 5. The variation of $R_2(1/\tau_{cp})$ as a function of $1/\tau_{cp}$ is called relaxation dispersion.

The chemical exchange contribution to transverse relaxation, R_{ex}, is defined as the difference between the apparent relaxation rate constants in the slow and fast pulsing limits:[19]

$$R_{ex} = \Delta R_2(0,\infty) = R_2(1/\tau_{cp} \rightarrow 0) - R_2(1/\tau_{cp} \rightarrow \infty) = {}^1/_2\left\{(\psi + \Delta\omega^2)^{1/2} - \frac{1}{\sqrt{2}}[\psi + (\psi^2 + \zeta^2)^{1/2}]^{1/2}\right\} \tag{8}$$

in which $\Delta R_2(1/\tau_{cp1},1/\tau_{cp2})$ is the difference between the transverse relaxation rate constants for two values of $1/\tau_{cp}$. Figure 1a presents calculated values of R_{ex} as a function of k_{ex} using eq 8, assuming $R_a = R_b$. The limiting values of R_{ex} in slow and fast exchange are

$$R_{ex} = p_b k_{ex} \qquad (k_{ex}/\Delta\omega \rightarrow 0) \tag{9}$$

$$R_{ex} = p_a p_b \Delta\omega^2 / k_{ex} \qquad (k_{ex}/\Delta\omega \rightarrow \infty) \tag{10}$$

respectively. The limiting results that R_{ex} depends quadratically on the static field strength for very fast exchange[21,23,24] and that R_{ex} is independent of the static field strength for very slow exchange[34] are known. The functional form of R_{ex} given by eq 8 is not overly sensitive to the values of R_a and R_b provided that $|R_a - R_b|/\Delta\omega \ll (p_a - p_b)$. In the case of interest herein, $p_a \gg p_b$ and assuming $R_a = R_b$:

$$R_{ex} \approx \frac{p_a p_b k_{ex}}{1 + (k_{ex}/\Delta\omega)^2} \tag{11}$$

For small changes in the static magnetic field, the fractional change in the chemical exchange broadening, $\delta R_{ex}/R_{ex}$, and the fractional change in the static field, $\delta B_0/B_0$, are related by

$$\frac{\delta R_{ex}}{R_{ex}} = \alpha\frac{\delta B_0}{B_0} \tag{12}$$

The constant of proportionality or scaling factor α is defined by

$$\alpha = \frac{d \ln R_{ex}}{d \ln \Delta\omega} \tag{13}$$

Provided that $p_a \gg p_b$, α satisfies the constraints $0 \le \alpha \le 2$, which generalizes the limiting cases of eqs 9−10. For example, using eqs 11 and 13,

$$\alpha = \frac{2(k_{ex}/\Delta\omega)^2}{1 + (k_{ex}/\Delta\omega)^2} \tag{14}$$

in the limit $p_a \rightarrow 1$. As shown by eq 14, α is a function only of $k_{ex}/\Delta\omega$ and therefore defines the NMR chemical shift time scale:

$$\begin{aligned} 0 \le \alpha < 1 &\quad \text{slow exchange} \\ \alpha = 1 &\quad \text{intermediate exchange} \\ 1 < \alpha \le 2 &\quad \text{fast exchange} \end{aligned} \tag{15}$$

Numerical calculations based on eqs 8 and 13, shown in Figure 1b, confirm the central result that the value of α is bounded between 0 and 2 and defines the chemical exchange kinetic regime provided that $p_a > 0.7$. Most importantly, eq 14 and Figure 1b indicate that the chemical shift time regime can be determined from the static field dependence of the exchange contribution to the transverse relaxation rate constant for the dominant line (site A) even if the population of site B is so low as to be unobservable in the slow exchange limit.

Determining R_{ex} experimentally using eq 8 requires measuring $R_2(1/\tau_{cp})$ over a wide range of τ_{cp} values, which may be difficult empirically, and requires extrapolation, usually by curve-fitting. An alternative approach is based on the static magnetic field dependence of $R_2(1/\tau_{cp})$ for two experimentally accessible values

(31) Jen, J. *J. Magn. Reson.* **1978**, *30*, 111−128.
(32) Meiboom, S. *J. Chem. Phys.* **1961**, *34*, 375−388.
(33) Deverell, C.; Morgan, R. E.; Strange, J. H. *Mol. Phys.* **1970**, *18*, 553−559.
(34) Ishima, R.; Torchia, D. A. *J. Biomol. NMR* **1999**, *15*, 369−372.

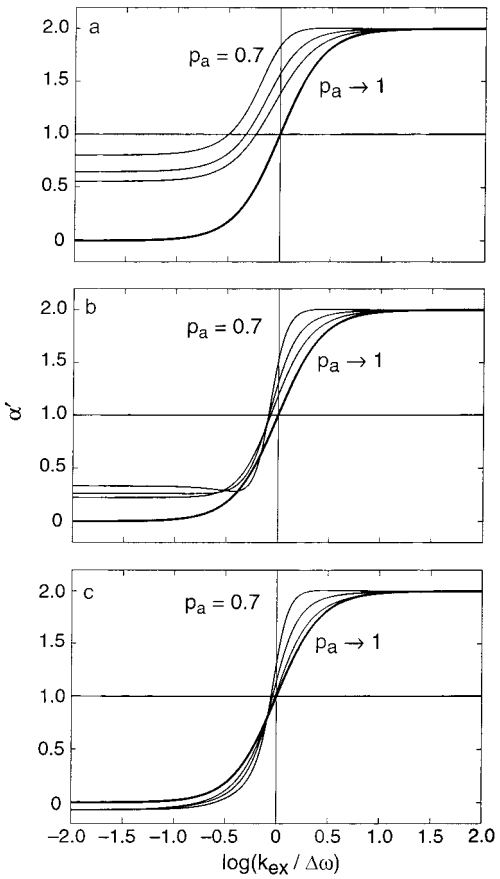

Figure 2. Comparison of α and α′. The limiting result for α as $p_a \rightarrow 1$ (eq 14) is shown as a heavy line. Values of α′, defined by eq 16, are shown as thin lines for site populations $p_a = 0.9$, 0.8, and 0.7. The results are calculated as functions of k_{ex}; the *x*-axis is normalized by $\Delta\omega$ for presentation. The slow exchange regime corresponds to $k_{ex}/\Delta\omega < 1$, and the fast exchange regime corresponds to $k_{ex}/\Delta\omega > 1$. Calculations were performed for values of $\Delta\omega$ equal to (a) 157 s^{-1} (25 Hz), (b) 314 s^{-1} (50 Hz), and (c) 628 s^{-1} (100 Hz). All calculations assumed $R_a = R_b$.

of τ_{cp}. In the present work, values of $R_2(1/\tau_{cp})$ for $\tau_{cp} = 64.5$ ms and $\tau_{cp} = 1.0$ ms were used to define

$$\alpha' = \mathrm{d} \ln \Delta R_2(0.016\ \mathrm{ms}^{-1}, 1.00\ \mathrm{ms}^{-1})/\mathrm{d} \ln \Delta\omega \quad (16)$$

As shown in Figure 2, α′ is a good approximation to α only if $p_a \gg p_b$ and $\Delta\omega$ is sufficiently large. However, a value of $\alpha' < 1$ is never observed if $k_{ex}/\Delta\omega > 1$. Therefore, a value of $\alpha' < 1$ always indicates that the system is in slow exchange, but a value of $\alpha' > 1$ does not definitively indicate the chemical shift time scale.

The complexity of eq 3 obfuscates the form of the dependence of $R_2(1/\tau_{cp})$ on $1/\tau_{cp}$. Ishima and Torchia have proposed a simple function that approximates eq 3 over all time scales provided $p_a \gg p_b$:[34]

$$R_2(1/\tau_{cp}) = R_2(1/\tau_{cp} \rightarrow \infty) + p_a p_b \Delta\omega^2 k_{ex}/[k_{ex}^2 + (p_a^2 \Delta\omega^4 + 144/\tau_{cp}^4)^{1/2}] \quad (17)$$

A simple measure of the τ_{cp}-dependence of relaxation dispersion is given by the value of $1/\tau_{cp}$ for which $R_2(1/\tau_{cp}) = [R_2(1/\tau_{cp} \rightarrow 0) + R_2(1/\tau_{cp} \rightarrow \infty)]/2$; this value will be defined as $1/\tau_{1/2}$. For eq 17,

$$1/\tau_{1/2} = \left(\frac{1}{12}\right)^{1/2} [(2p_a \Delta\omega^2 + k_{ex}^2)^2 - p_a^2 \Delta\omega^4]^{1/4} \quad (18)$$

The value of $1/\tau_{1/2}$, and therefore the decay profile of the relaxation dispersion curve, depends on the chemical shift time scale. In the limit of fast exchange, $k_{ex}/\Delta\omega \rightarrow \infty$, $1/\tau_{1/2} = k_{ex}/12^{1/2}$ is independent of the static magnetic field, and in the limit of slow exchange, $k_{ex}/\Delta\omega \rightarrow 0$, $1/\tau_{1/2} = \Delta\omega\ p_a^{1/2}/48^{1/4}$ depends linearly on the static magnetic field. Thus, if chemical exchange does not approach the fast limit, the decay of the relaxation dispersion curve is more gradual at higher static magnetic fields due to the increase in $\Delta\omega$. As discussed below, the field dependence of relaxation dispersion has important practical consequences for experimental investigations of chemical exchange in macromolecules.

Materials and Methods

The ^{15}N $R_2(1/\tau_{cp})$ measurements were performed at two static magnetic fields, $B_0 = 11.7$ T (corresponding to a proton Larmor frequency of 500.13 MHz) and 14.1 T (corresponding to a proton Larmor frequency of 600.13 MHz), and two temperatures, $T = 300$ K and 313 K, using a 2.6 mM BPTI (U-98% ^{15}N) sample in 90% H_2O/10% D_2O. Data were recorded at 11.7 T using a Bruker DRX-500 spectrometer and at 14.1 T using a Bruker DRX-600 spectrometer. Both spectrometers were equipped with triple-resonance three-axis gradient probeheads. Sample temperatures were calibrated using an 80% ethylene glycol sample in d_6-DMSO and a calibration curve provided by Bruker Instruments.

The relaxation-compensated CPMG pulse sequence[14] shown in Figure 3a was used to record CPMG experiments for most values of τ_{cp}. The conventional pulse sequence[35] for measuring ^{15}N R_2 shown in Figure 3b was used to record the CPMG experiments for values of $\tau_{cp} = 10.8$ ms and 21.5 ms. Both sequences average in-phase and antiphase coherences in order to eliminate any τ_{cp}-dependent effects arising from differential relaxation of these coherences and apply ^{1}H 180° pulses to eliminate ^{1}H−^{15}N dipolar/^{15}N chemical shift anisotropy relaxation interference.[36,37] In contrast to the sequence of Figure 3a, the sequence of Figure 3b begins with a refocused INEPT element to generate in-phase magnetization at the beginning of the CPMG period so that the ^{1}H 180° pulses used to eliminate relaxation interference are applied only when the ^{15}N coherence is in-phase. In the sequence of Figure 3a, the averaging of coherences is performed explicitly during the U period; in the sequence of Figure 3b, the averaging is performed implicitly by setting $\tau_{cp} = m/J_{NH}$, in which $J_{NH} = 93$ Hz is the average value of the one-bond ^{1}H−^{15}N scalar coupling constant and $m = 1$ or 2.[37] The sequence of Figure 3b is advantageous for values of $\tau_{cp} = 10.8$ ms and 21.5 ms because the first nonzero time point can be recorded at $2\tau_{cp}$ rather than $4\tau_{cp}$ as necessary for the sequence of Figure 3a. At each combination of τ_{cp}, T and B_0, $R_2(1/\tau_{cp})$ was determined from a time series in which $4n\tau_{cp}$ for the sequence of Figure 3a or $2n\tau_{cp}$ for the sequence of Figure 3b were varied between 0 and 320 ms by varying the integer n. Typically, 9−10 individual time points were recorded plus two duplicate time points. The time points for $n = 0$ were recorded by omitting the bracketed segments in Figure 3a and 3b.

The value of $R_2(1/\tau_{cp})$ for $\tau_{cp} = 64.5$ ms was obtained using the Hahn-echo pulse sequence shown in Figure 3c. Only two time points were recorded to determine the relaxation rate constant: one at zero time obtained with the bracketed segments omitted, and one at $\tau_{cp} = 64.5$ ms. The value of τ_{cp} was set to $6/J_{NH}$ to ensure that the ^{1}H 180°

(35) Farrow, N. A.; Zhang, O.; Forman-Kay, J. D.; Kay, L. E. *Biochemistry* **1995**, *34*, 868−878.
(36) Kay, L. E.; Nicholson, L. K.; Delaglio, F.; Bax, A.; Torchia, D. A. *J. Magn. Reson.* **1992**, *97*, 359−375.
(37) Palmer, A. G.; Skelton, N. J.; Chazin, W. J.; Wright, P. E.; Rance, M. *Mol. Phys.* **1992**, *75*, 699−711.

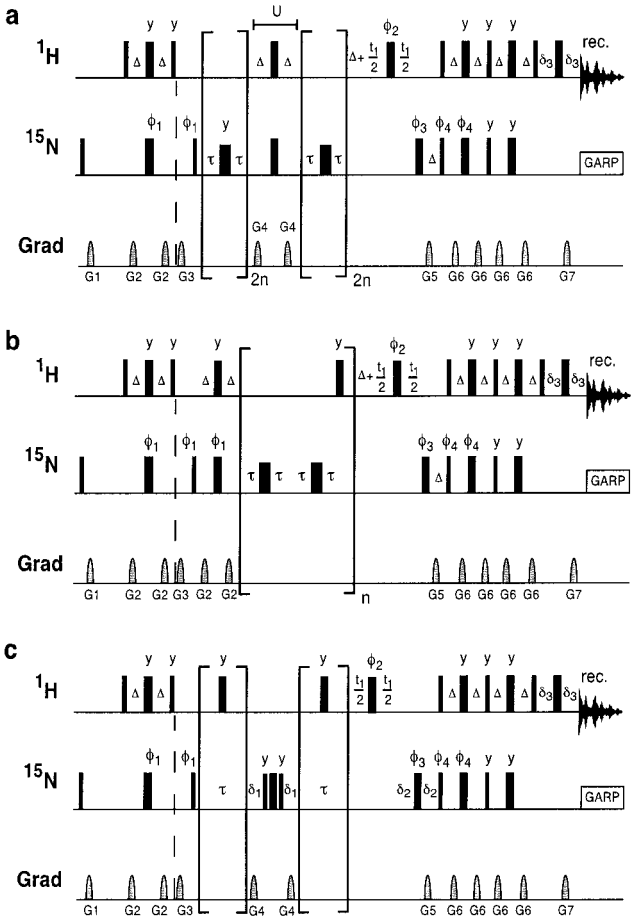

Figure 3. Pulse sequences for measuring ^{15}N $R_2(1/\tau_{cp})$. (a) Relaxation compensated CPMG experiment[14] for recording data with $\tau_{cp} < 10$ ms. (b) CPMG experiment for recording data with $\tau_{cp} = 10.8$ or 21.6 ms.[35] (c) Hahn-echo pulse sequence for recording data with $\tau_{cp} = 64.5$ ms. In (a), averaging of the relaxation rate constants for in-phase and antiphase coherences is performed by interchanging the coherences during U.[14] In (b), averaging is performed by setting $\tau_{cp} = m/J_{NH}$, in which m is an integer and J_{NH} is the one-bond ^{1}H$-^{15}$N scalar coupling constant;[37] $m = 1$ for $\tau_{cp} = 10.8$ ms and $m = 2$ for $\tau_{cp} = 21.6$ ms. In (c), averaging is performed by setting $\tau_{cp} = 2m/J_{NH}$; $m = 3$ for $\tau_{cp} = 64.5$ ms. Relaxation delays are (a) $t = 4n\tau_{cp}$ and (b) $t = 2n\tau_{cp}$, in which $n \geq 0$ is an integer; decay curves are obtained by recording a series of spectra for different values of n. In (c) spectra are recorded only at values of $t = 0$ and $t = \tau_{cp}$. Spectra for $t = 0$ are obtained by omitting the bracketed elements in (a$-$c). Narrow and wide bars depict 90° and 180° pulses, respectively. All pulses are x phase unless otherwise indicated. ^{15}N decoupling during acquisition was achieved with a 2 kHz GARP sequence.[51] Delays are $\tau = \tau_{cp}/2$, $\Delta = 2.7$ ms, $\delta_1 = 750$ μs, $\delta_2 = 2.05$ ms, $\delta_3 = 384$ μs. The phase cycle is $\phi_1 = x, -x$; $\phi_2 = 4(x), 4(-x)$; $\phi_3 = x, x, y, y, -x, -x, -y, -y$; $\phi_4 = x, -x$; receiver $= x, -x, -x, x$. The gradients are sine shaped with duration $G1-G7 = 1$, 0.4, 2, 0.5, 1.8, 0.6, and 0.184 ms and amplitude $G1_{xyz} = 8$; $G2_{xyz} = 6$; $G3_z = 15$; $G4_{xyz} = 7$; $G5_{xyz} = 24$; $G6_z = 21$; and $G7_{xyz} = 24$ G/cm. Coherence selection was achieved by inverting the amplitude of $G5$ and phase ϕ_4;[52] ϕ_1 and the receiver phases were inverted for each t_1 increment to shift axial peaks to the edge of the spectrum.[53]

pulses used to eliminate ^{1}H$-^{15}$N dipolar/^{15}N chemical shift anisotropy relaxation interference are applied when the ^{15}N coherences are in-phase. The zero time point must be acquired with the ^{1}H 180° pulses removed from the sequence; otherwise, these pulses would be applied to antiphase coherence, and imperfections in the pulses would lead to loss of signal intensity compared with spectra acquired with $\tau_{cp} = 64.5$ ms.

At a temperature of 300 K and $B_0 = 11.7$ T, data were recorded for τ_{cp} values of 1.0, 1.5, 2.0, 4.0, 6.6, 10.8, 21.5, and 64.5 ms; the data at $\tau_{cp} = 1.0$, 1.5, and 2.0 ms were reported earlier and used a variant of the pulse sequence in Figure 3a.[14] At each other combination of temperature and static field strength, data were collected for τ_{cp} values of 1.0, 1.5, 2.0, 4.0, 6.6, 10.8, and 65.4 ms.

Spectra were acquired using (128 × 2048) complex points and spectral widths of (2500 × 12500) Hz in the ($t_1 \times t_2$) dimensions. The ^{1}H carrier frequency was set coincident with the water resonance; the ^{15}N carrier frequency was set to 115.5 ppm. The recycle delay was 3 s. A total of 16 transients were recorded for each complex point for spectra recorded using the pulse sequences of Figure 3a and 3b. For the pulse sequence of Figure 3c, the spectrum at time zero was recorded with a total of 16 transients for each complex point while the spectrum at $\tau_{cp} = 65.4$ ms was recorded as 8 duplicate spectra with 16 transients per complex point. FELIX97 (MSI) was used for the processing of all spectra. The free induction decays were processed in F2 by applying a convolution filter to suppress the solvent signal, apodizing with an exponential window function, zero-filling once, and Fourier transforming. The resulting spectra were phase-corrected and baseline-corrected. The F1 interferograms were apodized with a Kaiser window function, zero-filled once, Fourier-transformed, and phase-corrected. Peak intensities were measured as the sum of the intensities for a 3 × 3 grid centered on the peak maxima.

Time series data obtained using Figure 3a and 3b were fit using the in-house program CurveFit to a monoexponential decay function, $I(t) = I(0)\exp[-R_2(1/\tau_{cp})t]$, in which $I(t)$ is the intensity of the resonance in the spectrum recorded at time $t = 4n\tau_{cp}$ or $t = 2n\tau_{cp}$ for data recorded with the sequence of Figure 3a or 3b, respectively. Experimental uncertainties in the peak intensities were estimated from duplicate spectra.[38,39] Uncertainties in the fitted rate constants were obtained from jackknife simulations.[40] For the Hahn-echo experiment of Figure 3c, rate constants were obtained from $R_2(1/\tau_{cp}) = \ln[I(0)/\langle I(\tau_{cp})\rangle]/\tau_{cp}$, in which $\tau_{cp} = 64.5$ ms, $I(0)$ is the intensity in the spectrum recorded with a relaxation delay of zero, and $\langle I(\tau_{cp})\rangle$ is the trimmed mean intensity calculated after eliminating the maximum and minimum intensities from the 8 spectra recorded at the nonzero relaxation delay. Uncertainties in $\langle I(\tau_{cp})\rangle$ were taken to be the standard error in the trimmed mean. $I(0)$ was assumed to have the same relative uncertainty as the trimmed set of $I(\tau_{cp})$ values. The experimental uncertainties in $R_2(1/\tau_{cp})$ determined by this method were confirmed by recording duplicate data sets at $T =$ 313 K and $B_0 = 11.7$ T and at $T = 300$ K and $B_0 = 14.1$ T.

Dispersion curves for $R_2(1/\tau_{cp})$ were fit to eq 3 or to the fast-limit formula:[41]

$$R_2(1/\tau_{cp}) = R_2(1/\tau_{cp} \rightarrow \infty) + R_{ex}[1 - 2\tanh(k_{ex}\tau_{cp}/2)/(k_{ex}\tau_{cp})] \quad (19)$$

All data points were weighted equally in performing the curve-fitting, using the mean uncertainty for the $R_2(1/\tau_{cp})$ values in the dispersion curve and uncertainties in fitted parameters were obtained from jackknife simulations. The value of $R_2(1/\tau_{cp} \rightarrow \infty)$ obtained from the pulse sequences in Figure 3 is the average of the relaxation rate constants for in-phase and antiphase ^{15}N magnetization.[14]

Values of α were calculated from values of R_{ex} measured for two values of B_0 using the following expression:

$$\alpha = \left(\frac{B_{02} + B_{01}}{B_{02} - B_{01}}\right)\left(\frac{R_{ex2} - R_{ex1}}{R_{ex2} + R_{ex1}}\right) \quad (20)$$

in which R_{ex1} and R_{ex2} are the values measured at the lower field, B_{01} (11.7 T) and the higher field, B_{02} (14.1 T). The value of α calculated by eq 20 is a numerical approximation to eq 13 and is associated with an effective field $(B_{01} + B_{02})/2$. Values of α′ were obtained by substituting $\Delta R_2(0.016\ \text{ms}^{-1}, 1.00\ \text{ms}^{-1})$ for R_{ex} in eq 20. Uncertainties

(38) Palmer, A. G.; Rance, M.; Wright, P. E. *J. Am. Chem. Soc.* **1991**, *113*, 4371−4380.
(39) Skelton, N. J.; Palmer, A. G.; Akke, M.; Kördel, J.; Rance, M.; Chazin, W. J. *J. Magn. Reson., Ser. B* **1993**, *102*, 253−264.
(40) Mosteller, F.; Tukey, J. W. *Data Analysis and Regression. A Second Course in Statistics*; Addison-Wesley: Reading, MA, 1977.
(41) Luz, Z.; Meiboom, S. *J. Chem. Phys.* **1963**, *39*, 366−370.

in α and α′ were obtained by propagation of the uncertainties in R_{ex} and ΔR_2(0.016 ms^{-1}, 1.00 ms^{-1}), respectively.

Results

Backbone amide ^{15}N spin relaxation rate constants were determined for 44 residues in BPTI whose resonances were not overlapped in the two-dimensional ^{1}H−^{15}N correlation spectra at any of the temperatures (300 and 313 K) or fields (11.7 and 14.1 T) used. All measured rate constants are provided in Supporting Information. Backbone amide assignments were taken from Glushka et al.[42]

Relaxation rate constants were recorded using three different pulse sequences, shown in Figure 3, to obtain the widest range of τ_{cp} values with optimal sensitivity. The average experimental uncertainty for the experiments of a, b, and c in Figure 3 averaged over all combinations of temperature and static field strengths were 0.10, 0.09, and 0.33 s^{-1}, respectively. A series of control experiments were performed to ensure that relaxation rate constants obtained from the different experimental methods were commensurate. Both a and b in Figure 3 are CPMG experiments; however, different strategies are used for averaging the relaxation contributions from in-phase and antiphase coherences. The accuracy of the experiment of Figure 3b relative to the experiment of Figure 3a was assessed by recording a second relaxation curve at T = 300 K and B_0 = 11.7 T using the experiment of Figure 3a and τ_{cp} = 10.8 ms. The mean pairwise deviation between the data recorded using a and b in Figure 3 was 0.16 s^{-1} with a standard deviation of 0.29 s^{-1}. The value of $R_2(1/\tau_{cp})$ for the smallest value of $1/\tau_{cp}$ (τ_{cp} = 64.5 ms) was obtained with the Hahn echo sequence of Figure 3c as opposed to the CPMG sequences of a and b of Figure 3. The reproducibility of the Hahn echo experiment was assessed by calculating paired differences between duplicate spectra. For data recorded at T = 300 K and B_0 = 14.1 T, the mean difference was 0.17 s^{-1} with a standard deviation of 0.15 s^{-1}. The standard deviation divided by $2^{1/2}$ agrees well with the average experimental uncertainty of 0.08 s^{-1} obtained by the error analysis method described in Materials and Methods. For data recorded at T = 313 K and B_0 = 11.7 T, the mean difference was 0.06 s^{-1} with a standard deviation of 0.25 s^{-1}. The standard deviation divided by $2^{1/2}$ agrees well with the average experimental uncertainty of 0.15 s^{-1}. The accuracy of the Hahn echo experiment was tested by comparing the relaxation rate constants obtained using b and c of Figurs 3. The mean difference, $R_2(1/\tau_{cp} = 0.016\ \text{ms}^{-1}) - R_2(1/\tau_{cp} = 0.092\ \text{ms}^{-1})$ was 0.44 ± 0.45 s^{-1} averaged over all residues not subject to conformational exchange linebroadening (for this calculation, residues 12−18 and 35−42 were excluded as potentially subject to exchange effects).

The majority of backbone ^{15}N sites in BPTI are not subject to chemical exchange processes, and the relaxation rate constants $R_2(1/\tau_{cp})$ were independent of τ_{cp} and of the pulse sequences used to measure $R_2(1/\tau_{cp})$. This result is illustrated in Figure 4 for Gln31. The standard deviation of all $R_2(1/\tau_{cp})$ values with respect to the mean value for each residue at each temperature and static field strength was 0.28 s^{-1}. This value represents both the within-experiment and experiment-to-experiment variability and is 1−3-fold larger than the random uncertainty associated with individual relaxation rate constants recorded for individual values of τ_{cp} given above.

Strong dependence of $R_2(1/\tau_{cp})$ on $1/\tau_{cp}$ is observed for residues in the vicinity of the Cys14−Cys38 disulfide bond in

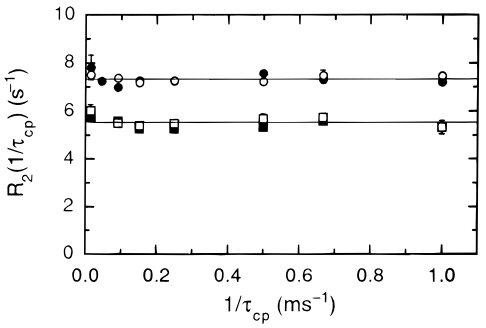

Figure 4. Relaxation rate constants for Gln31. Values of $R_2(1/\tau_{cp})$ are shown for (●) T = 300 K, B_0 = 11.7 T; (○) T = 300 K, B_0 = 14.1 T; (■) T = 313 K, B_0 = 11.7 T; and (□) T = 313 K, B_0 = 14.1 T. Lines are drawn at the average values of the rate constants at 300 K and at 313 K, 7.34 s^{-1} and 5.51 s^{-1}, respectively and simply serve to guide the eye. Small differences between relaxation rate constants at 11.7 and 14.1 T arise from field dependence of chemical shift anisotropy. The average uncertainty in the relaxation rate constants is 0.12 s^{-1}, and the average standard deviation for the relaxation rate constants with respect to the average values is 0.21 s^{-1}. The former reflects within-experiment variation and the latter reflects both within-experiment and between-experiment variation.

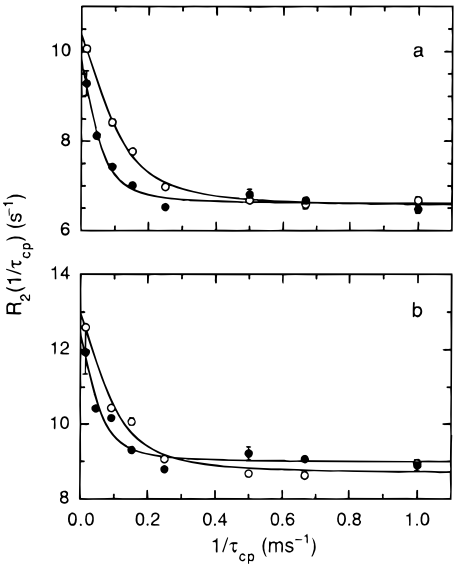

Figure 5. Relaxation dispersion curves for (a) Ala16 and (b) Gly36 at 300 K. Values of $R_2(1/\tau_{cp})$ at (●) B_0 = 11.7 T and (○) B_0 = 14.1 T are shown for each residue. The lines are the best fit of eq 19 to the data. Fitted parameters are given in Table 1.

BPTI, including residues Ala16, Gly36, Cys38, Arg39, and Ala40. As discussed previously, residues Cys14 and Lys15 are subject to exchange broadening, but decay of the relaxation dispersion curves was not observed in the present experiments.[14] To obtain estimates of R_{ex}, dispersion curves recorded for each combination of temperature and static magnetic field strength were fit independently. In most cases, eq 19, the fast-limit approximation, gave adequate fits to the experimental data, and the full form of eq 3, which requires an additional adjustable parameter, offered no advantages. However, the relaxation dispersion curves for Arg39 at T = 300 K could not be fit acceptably by eq 19 and the dispersion curves were fit with eq 3. Dispersion curves are shown in Figure 5 for Ala16 and Gly36 at T = 300 K. R_{ex} values for Ala16 and Gly36 were <2 s^{-1} at 313 K and could not be measured with sufficient precision for determination of α; dispersion curves for these residues at 313 K are not shown. Dispersion curves at T = 300 and 313 K for residues Cys38, Arg39, and Ala40 are shown in Figures 6−8,

(42) Glushka, J.; Lee, M.; Coffin, S.; Cowburn, D. *J. Am. Chem. Soc.* **1989**, *111*, 7716−7722.

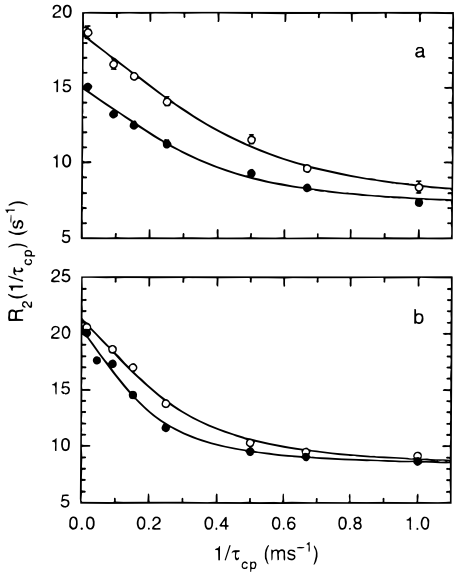

Figure 6. Relaxation dispersion curves for Cys38 at (a) 313 K and (b) 300 K. Values of $R_2(1/\tau_{cp})$ at (●) $B_0 = 11.7$ T and (○) $B_0 = 14.1$ T are shown at each temperature. The lines are the best fit of eq 19 to the data. Fitted parameters are given in Tables 1 and 2.

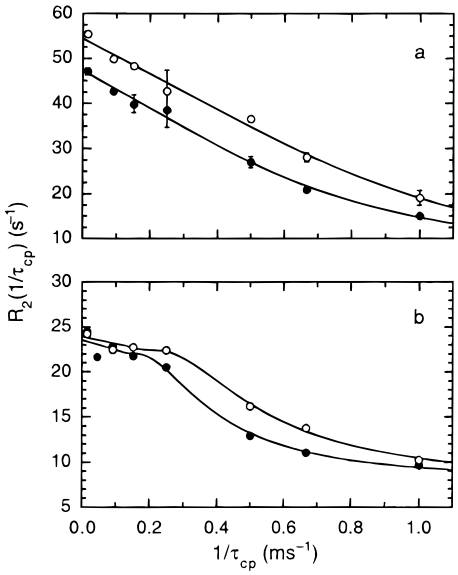

Figure 7. Relaxation dispersion curves for Arg39 at (a) 313 K and (b) 300 K. Values of $R_2(1/\tau_{cp})$ at (●) $B_0 = 11.7$ T and (○) $B_0 = 14.1$ T are shown at each temperature. In (a) the lines are the best fit of eq 19 and fitted parameters are given in Table 2. In (b) the lines are the best fit of eq 3 and fitted parameters are given in Table 1.

respectively. The relaxation dispersion curves for Arg39 at $T = 313$ K do not define the value of $R_2(1/\tau_{cp} \rightarrow \infty)$ due to experimental limitations on the maximum value of $1/\tau_{cp}$. Accordingly, fitting of the dispersion curves assumed values of $R_2(1/\tau_{cp} \rightarrow \infty) = 7.0$ s^{-1} at $T = 313$ K. Variations in the assumed limiting value by ± 2 s^{-1} changed α by ± 0.04, a variation less than the overall uncertainty. Fitted values of R_{ex}, $1/\tau_{1/2}$, and $R_2(1/\tau_{cp} \rightarrow \infty)$ are given in Table 1 for $T = 300$ K and in Table 2 for $T = 313$ K. At each temperature studied, the data recorded at the two static magnetic fields yield very similar values of $R_2(1/\tau_{cp} \rightarrow \infty)$; a slight increase in the limiting value at $B_0 = 14.1$ T is due to the field dependence of chemical shift anisotropy. The values of $1/\tau_{1/2}$ obtained from fitting either eqs 3 or 19 to the dispersion curves are somewhat larger at 14.1 T than 11.7 T for most residues. As predicted by eq 18, an increase

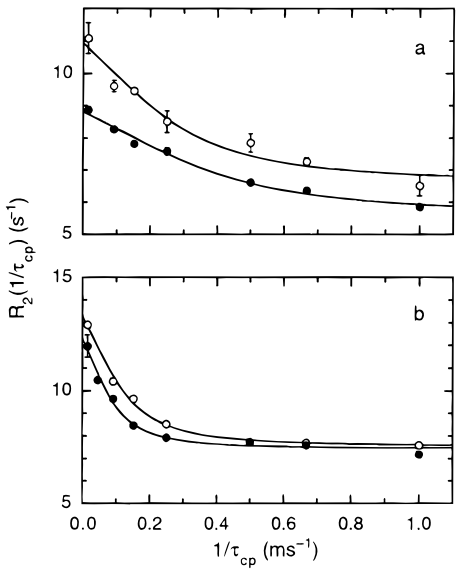

Figure 8. Relaxation dispersion curves for Ala40 at (a) 313 K and (b) 300 K. Values of $R_2(1/\tau_{cp})$ at (●) $B_0 = 11.7$ T and (○) $B_0 = 14.1$ T are shown at each temperature. The lines are the best fit of eq 19 to the data. Fitted parameters are given in Tables 1 and 2.

Table 1. Relaxation Dispersion Parameters for BPTI at 300 K[a]

residue	B_0 (T)	R_{ex} (s^{-1})	$1/\tau_{1/2}$ (s^{-1})	$R_2(1/\tau_{cp} \rightarrow \infty)$ (s^{-1})
Ala16	11.7	3.22 ± 0.16	46 ± 3	6.60 ± 0.06
	14.1	3.85 ± 0.08	92 ± 2	6.54 ± 0.04
Gly36	11.7	3.47 ± 0.26	47 ± 5	8.98 ± 0.09
	14.1	4.32 ± 0.08	82 ± 2	8.68 ± 0.04
Cys38	11.7	12.13 ± 0.15	156 ± 3	8.26 ± 0.11
	14.1	13.22 ± 0.13	221 ± 4	8.11 ± 0.11
Arg39[b]	11.7	15.74 ± 0.36	389 ± 6	7.78 ± 0.30
	14.1	16.50 ± 0.36	536 ± 8	7.41 ± 0.32
Ala40	11.7	4.92 ± 0.18	76 ± 4	7.43 ± 0.08
	14.1	5.77 ± 0.10	102 ± 2	7.53 ± 0.05

[a] Parameters were obtained by fitting eq 19 to the $R_2(1/\tau_{cp})$ relaxation dispersion data, unless otherwise indicated. [b] Parameters were obtained by fitting eq 3 to the $R_2(1/\tau_{cp})$ relaxation dispersion data.

Table 2. Relaxation Dispersion Parameters for BPTI at 313 K[a]

residue	B_0 (T)	R_{ex} (s^{-1})	$1/\tau_{1/2}$ (s^{-1})	$R_2(1/\tau_{cp} \rightarrow \infty)$ (s^{-1})
Ala16[b]	11.7	1.12 ± 0.08	79 ± 8	4.90 ± 0.03
Gly36	11.7	1.24 ± 0.10	168 ± 24	6.53 ± 0.08
	14.1	1.67 ± 0.23	172 ± 36	6.80 ± 0.18
Cys38	11.7	8.03 ± 0.17	272 ± 10	6.95 ± 0.17
	14.1	11.52 ± 0.47	350 ± 24	7.00 ± 0.51
Arg39	11.7	40.5 ± 0.8	480 ± 12	[7][c]
	14.1	47.8 ± 0.9	585 ± 13	[7][c]
Ala40	11.7	3.24 ± 0.11	318 ± 19	5.58 ± 0.12
	14.1	4.34 ± 0.30	227 ± 29	6.60 ± 0.28

[a] Parameters were obtained by fitting eq 19 to the $R_2(1/\tau_{cp})$ relaxation dispersion data. [b] Dispersion data could not be analyzed for Ala16 at 14.1 T due to limited precision of the fitted $R_2(1/\tau_{cp})$ values. [c] The value of $R_2(1/\tau_{cp} \rightarrow \infty)$ was fixed at 7 s^{-1}.

in $1/\tau_{1/2}$ at large fields is indicative of chemical exchange processes outside the fast limit. Values of α and α' determined from the relaxation data are given in Table 3.

Dispersion curves recorded at static magnetic fields of 11.7 and 14.1 T for Cys38 and Arg39 also were fit globally. In these analyses, $\Delta\omega$ was scaled linearly with B_0, while other fitting parameters were assumed to be independent of the field (the small field dependence of $R_2(1/\tau_{cp} \rightarrow \infty)$ was not considered for simplicity). The measured values of α indicate that Cys38 at $T = 300$ K, Arg39 at $T = 300$ K, and Arg39 at $T = 313$ K are subject to exchange that is slow to intermediate on the

Table 3. Scaling Factors α and α′ for BPTI

	$T = 300$ K		$T = 313$ K	
residue	α	α′	α	α′
Ala16	0.98 ± 0.29	1.0 ± 0.6	N.A.[a]	N.A.
Gly36	1.2 ± 0.4	N.A.	N.A.	N A.
Cys38	0.47 ± 0.09	0.02 ± 0.23	1.96 ± 0.25	1.6 ± 0.3
Arg39	0.26 ± 0.17	-0.34 ± 0.22	0.91 ± 0.15	0.7 ± 0.3
Ala40	0.87 ± 0.31	0.6 ± 0.6	1.6 ± 0.4	2.2 ± 0.7

[a] Not Available. Values of α or α′ are reported only if the uncertainty in the value is <0.8.

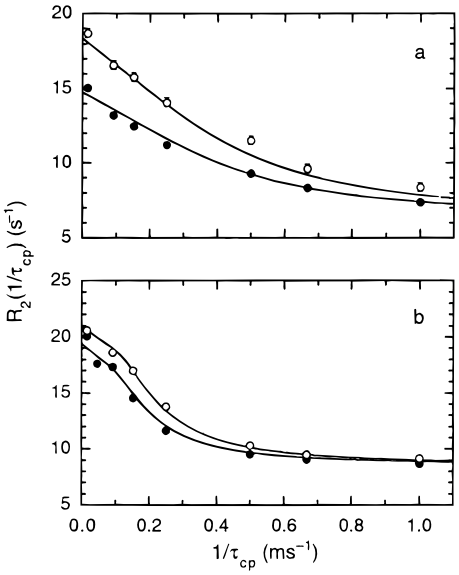

Figure 9. Global analysis of relaxation dispersion curves for Cys38 at (a) 313 K and (b) 300 K. Values of $R_2(1/\tau_{cp})$ at (●) $B_0 = 11.7$ T and (○) $B_0 = 14.1$ T are shown at each temperature. In (a) the lines are the best simultaneous fit of eq 19 to data recorded at $B_0 = 11.7$ and 14.1 T; in (b) the lines are the best simultaneous fit of eq 3. Fitted parameters are given in Table 4.

chemical shift time scale. In accordance with these results, at least a 5-fold reduction of the residual χ^2 statistic was obtained using eq 3 compared with the fast-limit result of eq 19 when performing global fits. In contrast, α indicates that exchange for Cys38 approaches the fast limit at $T = 313$ K and nearly identical global fits were obtained using eqs 3 and 19. Fitted dispersion curves for Cys38 and Arg39 are shown in Figures 9 and 10, respectively. Fitted parameters are given in Table 4. Values of R_{ex} were at least 2-fold greater for Cys38 and Arg39 than for other residues in BPTI, and global fits to residues with $R_{ex} < 6$ s^{-1} were less successful.

Discussion

Detailed analyses of chemical exchange linebroadening effects to determine kinetic rate constants rely on curve-fitting of appropriate functional forms to experimental data. In most instances, if a single exchange broadened resonance is observed for a nuclear spin, fast limit chemical exchange is assumed to be applicable with a quadratic dependence on the static magnetic field strength.[21−24] In contrast to these usual suppositions, the major result of the present work is that R_{ex} depends on the static magnetic field strength through the scaling relationship $\delta R_{ex}/R_{ex} = \alpha(\delta B_0/B_0)$, in which $0 \le \alpha \le 2$ for $p_a > 0.7$. The value of α depends on the NMR chemical shift time scale for the exchange process. Quadratic dependence of R_{ex} on the static magnetic field strength is observed only for very fast limit exchange in which $\alpha \rightarrow 2$. R_{ex} is independent of the static magnetic field strength for very slow exchange in which $\alpha \rightarrow 0$. If the site populations for a spin subject to chemical exchange are highly skewed, the resonance for the minor population can be unobservable even in slow exchange; thus, mere observation of a single exchange-broadened resonance does not confirm that exchange is in the fast limit. Nonetheless, the scaling factor α for the more highly populated site A defines the chemical shift time scale for a chemical exchange process even for highly skewed site populations.

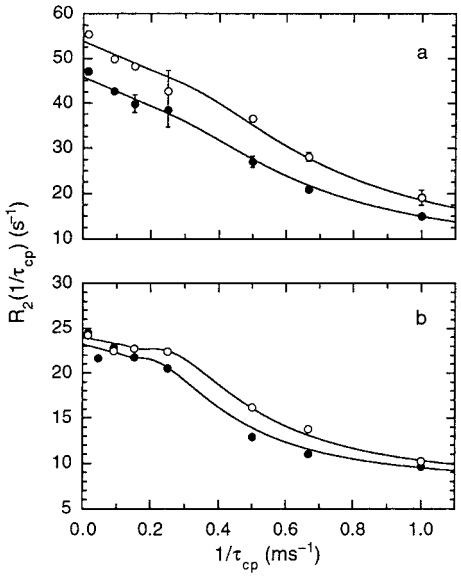

Figure 10. Global analysis of relaxation dispersion curves for Arg39 at (a) 313 K and (b) 300 K. Values of $R_2(1/\tau_{cp})$ at (●) $B_0 = 11.7$ T and (○) $B_0 = 14.1$ T are shown at each temperature. The lines are the best simultaneous fit of eq 3 to data recorded at $B_0 = 11.7$ and 14.1 T and fitted parameters are given in Table 4.

Table 4. Chemical Exchange Parameters for Cys38 and Arg39 in BPTI[a]

residue	T (K)	p_a	$\Delta\omega$ (s^{-1})[b]	k_{ex} (s^{-1})	$R_2(1/\tau_{cp})$ (s^{-1})
Cys38	300	0.953 ± 0.004	452 ± 20	380 ± 70	8.6 ± 0.1
	310[c]	0.944 ± 0.014	N.A.	1300 ± 290	6.4 ± 0.7
Arg39	300	0.965 ± 0.004	1180 ± 50	530 ± 90	7.6 ± 0.3
	310	0.940 ± 0.006	1280 ± 160	1370 ± 160	6.4 ± 2.4

[a] Results obtained by simultaneously fitting eq 3 to $R_2(1/\tau_{cp})$ dispersion curves recorded at 11.7 and 14.1 T, unless otherwise indicated. [b] $\Delta\omega$ is reported for $B_0 = 11.7$ T. [c] Results for Cys38 at 313 K were obtained by fitting eq 19 to $R_2(1/\tau_{cp})$ dispersion curves recorded at 11.7 and 14.1 T. The value of p_a was obtained from eq 10 assuming $\Delta\omega$ was unchanged from the value obtained at 300 K.

Herein, α was calculated using the numerical approximation given in eq 20 for R_{ex} values measured at two static magnetic field strengths. As shown by this equation, α is a function of the ratio of the exchange contributions at the two fields, R_{ex2}/R_{ex1}. Thus, this ratio also can be used to characterize the chemical shift time scale because $1 \le R_{ex2}/R_{ex1} < B_{02}/B_{01}$ for slow exchange, $R_{ex2}/R_{ex1} = B_{02}/B_{01}$ for intermediate exchange, and $B_{02}/B_{01} < R_{ex2}/R_{ex1} \le (B_{02}/B_{01})^2$ for fast exchange. However, α has two advantages compared with R_{ex2}/R_{ex1} for characterizing chemical exchange: first, α has a fundamental mathematical definition and physical interpretation given by eq 12, and second, α has a range of values that is independent of the static magnetic field strengths used to measure R_{ex1} and R_{ex2}.

Use of the three pulse sequences shown in Figure 3 were necessary to access the widest possible range of τ_{cp} values with optimal sensitivity. Pulse sequences employed in the present work to measure $R_2(1/\tau_{cp})$ average the relaxation rate constants

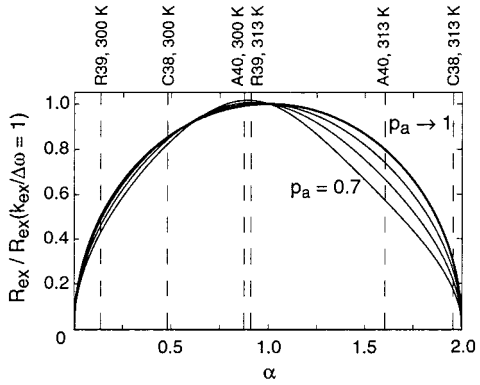

Figure 11. Temperature dependence of R_{ex} and α for BPTI. The values of R_{ex}, calculated from eq 8 are plotted versus α, calculated from eq 13. This graph is a transformation of Figure 1a and illustrates the dependence of R_{ex} on α. The slow exchange regime corresponds to $0 \leq \alpha < 1$, and the fast exchange regime corresponds to $1 < \alpha \leq 2$. Values of R_{ex} are normalized by the value at coalescence ($\alpha = 1$). Curves are drawn for site populations $p_a \rightarrow 1$ (heavy line), 0.9, 0.8, and 0.7. Calculations were performed assuming $R_a = R_b$ and $\Delta\omega = 628\ s^{-1}$ (100 Hz), but the shapes of the resulting curves depend weakly on these assumptions. The results for α with $p_a \rightarrow 1$ are essentially identical to eq 14. The experimentally determined values of α for Cys38, Arg39, and Ala40 at $T = 300$ K and $T = 313$ K, taken from Table 3, are indicated by dashed vertical lines to illustrate the different positions on the NMR chemical shift time scale exhibited by the ^{15}N spins of these residues in BPTI at the two temperatures.

for antiphase and in-phase coherences in order to remove any τ_{cp}-dependent effects arising from the difference between the relaxation rates of these two coherences.[37,14] Because antiphase relaxation usually is substantially larger than in-phase relaxation due to a contribution from proton−proton dipolar relaxation, these sequences suffer in sensitivity for larger proteins. Transverse relaxation optimized spectroscopy (TROSY),[43] based on the interference between chemical shift anisotropy and dipolar relaxation mechanisms, has been used to develop a variant of the pulse sequence of Figure 3a that performs substantially better for larger molecules.[44] Similar TROSY-based variants of the pulse sequences given in b and c of Figure 3 can be designed using the same approach.

The NMR chemical shift time scale depends on both k_{ex} and $\Delta\omega$; consequently, the same kinetic process can be manifested in different motional regimes for different nuclear spins, depending on the magnitude of $\Delta\omega$. In agreement with this observation, a range of motional properties are observed for the residues subject to conformational exchange broadening in BPTI at the two temperatures studied. The relationship between chemical exchange linebroadening and the NMR chemical shift time scale for Cys38, Arg39, and Ala40 is illustrated graphically in Figure 11. This figure depicts the dependence of R_{ex} on α and represents a transformation of the independent variable of Figure 1a. Cys38 was in slow exchange at 300 K and fast exchange at 313 K. Ala40 was close to coalescence at 300 K and in fast exchange at 313 K. In contrast, Arg39 was in slow exchange at 300 K and close to coalescence at 313 K; the dramatic increase in R_{ex} for Arg39 from $\sim 15\ s^{-1}$ at 300 K to $> 40\ s^{-1}$ at 313 K results from the near-coalescence conditions at 313 K. Ala16 and Gly36 were close to coalescence at 300 K, at which point R_{ex} is maximal, and the reduction in R_{ex} to very small values, $< 2\ s^{-1}$, at 313 K (Table 2) is consistent with a shift to fast exchange even though α could not be measured precisely for these residues at $T = 313$ K.

As shown by Figure 1a, a given value of R_{ex} can arise from either slow or fast chemical exchange on the NMR chemical shift time scale. Thus, a single measured value of R_{ex} cannot be used to ascertain the NMR time scale. This point is illustrated by the results for Cys38 at $B_0 = 14.1$ T. Very similar values of $R_{ex} = 13.22 \pm 0.13\ s^{-1}$ at 300 K and $R_{ex} = 11.5 \pm 0.5\ s^{-1}$ at 313 K are observed. Nonetheless, the very different values of $\alpha = 0.47 \pm 0.09$ at 300 K and $\alpha = 1.96 \pm 0.25$ at 313 K clearly demonstrate that chemical exchange is slow at 300 K and fast at 313 K. The temperature dependence of R_{ex} can be used in some circumstances to determine the time scale of chemical exchange.[45] An increase in temperature will increase k_{ex} through the Arrhenius equation and shift $k_{ex}/\Delta\omega$ toward larger values. Thus, as shown by Figure 1a, R_{ex} will increase with temperature if the exchange process is in the slow limit (Arg39 for example) and decrease with temperature if the exchange process is in the fast limit (Ala40). Unfortunately, temperature changes also perturb the site populations p_a and p_b through the Boltzmann equation, can affect $\Delta\omega$ through temperature-dependent conformational changes, and can be incompatible with sample stability. The use of the static magnetic field dependence of R_{ex} to determine α does not suffer from any of these limitations.

In principle, curve-fitting of the relaxation dispersion curve with functional forms applicable to all time scales (eqs 3 or 17, for example) can be used to determine whether a given exchange process is fast or slow on the NMR chemical shift time scale.[34] At 300 K, the chemical exchange processes for the ^{15}N amide spin of Cys38, Arg39, and Ala40 were in slow exchange with $\alpha < 1$, while the ^{15}N spin of Ala16 and Gly36 were close to coalescence with $\alpha \approx 1$. Nonetheless, only Arg39 displayed a relaxation dispersion curve that deviated substantially from the functional form assumed for fast limit exchange (eq 19). Thus, for the majority of the exchange-broadened sites in BPTI, curve-fitting relaxation dispersion data acquired at a single magnetic field strength cannot distinguish the fast and slow exchange regimes.

In the present case, R_{ex} was determined by extrapolating the relaxation dispersion curves to $1/\tau_{cp} = 0$ and $1/\tau_{cp} \rightarrow \infty$. This procedure requires acquisition of relaxation decay curves for a large number of τ_{cp} values, which is time-consuming experimentally. As shown by Figure 2 and Table 3, values of α' measured from the difference in $R_2(1/\tau_{cp})$ measured at one long and one short value of τ_{cp} are useful, but imperfect, indicators of the NMR time scale. A value of $\alpha' < 1$ is definitive evidence for slow exchange; however, a value of $\alpha' > 1$ does not distinguish between fast and slow exchange. This approach also does not require fitting a functional form to the dispersion curve and consequently is applicable to cases, such as Arg39, in which the dispersion curve is difficult to fit. A practical approach is to first measure R_{ex} for the longest and shortest experimentally achievable values of τ_{cp} and calculate α'. The full dispersion curve then only needs to be measured if α' is found to be greater than unity.

The principal shortcoming in determining α' is obtaining an estimate of $R_2(1/\tau_{cp} \rightarrow \infty)$ due to experimental limitations on the minimum value of τ_{cp}. As indicated by eq 18, outside of the fast exchange limit, the decay of the relaxation dispersion curve is slower at higher static magnetic field. Consequently, the value of $R_2(1.00\ ms^{-1})$ at $B_0 = 14.1$ T generally is larger

(43) Pervushin, K.; Riek, R.; Wider, G.; Wüthrich, K. *Proc. Natl. Acad. Sci. U.S.A.* **1997**, *94*, 12366−12371.

(44) Loria, J. P.; Rance, M.; Palmer, A. G. *J. Biomol. NMR* **1999**, *15*, 151−155.

(45) Mandel, A. M.; Akke, M.; Palmer, A. G. *Biochemistry* **1996**, *35*, 16009−16023.

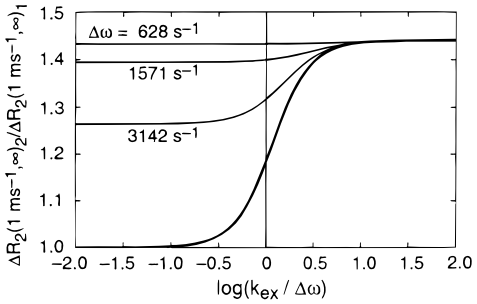

Figure 12. Chemical exchange for fast pulsing in CPMG experiments. The apparent exchange contribution to transverse relaxation for fast pulsing with $\tau_{cp} = 1$ ms is defined as $\Delta R_2(1\ ms^{-1},\infty) = R_2(1\ ms^{-1}) - R_2(1/\tau_{cp} \rightarrow \infty)$, and is calculated using eq 3. The thin lines depict the ratio $\Delta R_2(1\ ms^{-1},\infty)_2/\Delta R_2(1\ ms^{-1},\infty)_1$, in which $\Delta R_2(1\ ms^{-1})_1$ and $\Delta R_2(1\ ms^{-1})_2$ are calculated for $B_0 = 11.7$ T and $B_0 = 14.1$ T, respectively. Each line is labeled with the value of $\Delta\omega = 628$, 1571, and 3142 s^{-1}, used in the calculation for $B_0 = 11.7$ T; $\Delta\omega$ was scaled by a factor (14.1/11.7) for calculations at $B_0 = 14.1$ T. The heavy line depicts the ideal ratio R_{ex2}/R_{ex1}, in which R_{ex2} and R_{ex1} are calculated using eq 8 for $B_0 = 14.1$ T and $B_0 = 11.7$ T, respectively. The results are presented as functions of k_{ex}; the *x*-axis is normalized by $\Delta\omega$ for presentation The slow exchange regime corresponds to $k_{ex}/\Delta\omega < 1$, and the fast exchange regime corresponds to $k_{ex}/\Delta\omega > 1$. Calculations were performed assuming $R_a = R_b$ and $p_a = 0.95$, but the results depend weakly on these assumptions.

than at $B_0 = 11.7$ T, and $\Delta R_2(0.016\ ms^{-1},1.00\ ms^{-1})$ will be underestimated at $B_0 = 14.1$ T compared with $B_0 = 11.7$ T. Improved estimates of α' are obtained by using $R_2(1.00\ ms^{-1})$ measured at $B_0 = 11.7$ T for calculating $\Delta R_2(0.016\ ms^{-1},1.00\ ms^{-1})$ at both values of B_0. For example, values of α' calculated by this approach for Cys38 and Arg39 are 0.24 ± 0.23 and -0.10 ± 0.20 at $T = 300$ K and 2.10 ± 0.20 and 1.27 ± 0.16 at $T = 313$ K, respectively, and agree better with values of α given in Table 3. Relaxation interference experiments also can be used to obtain an estimate of the transverse relaxation rate constant for in-phase coherences that does not contain contributions from chemical exchange effects.[46,47] To first approximation, the average relaxation rate constant for in-phase and antiphase coherences is the in-phase relaxation rate constant plus one-half of the amide proton longitudinal relaxation rate constant. Combining relaxation interference experiments with experiments for measuring the amide proton longitudinal relaxation[48] may provide an alternative approach for obtaining $R_2(1/\tau_{cp} \rightarrow \infty)$ for determination of α'.

Most investigations of molecular dynamic properties of macromolecules using spin relaxation measure the transverse relaxation rate constant using CPMG experiments with a single value of $1/\tau_{cp} \geq 1\ ms^{-1}$.[5] In some of these studies, quadratic field dependence of the exchange contribution to $R_2(1/\tau_{cp})$ has been observed and taken as evidence for fast-limit chemical exchange kinetics.[21,23,24] However, the different τ_{cp}-dependence of the dispersion curves predicted by eq 18 for slow and fast chemical exchange complicates the interpretation of such measurements. Figure 12 compares the static magnetic field dependence of R_{ex} given by eq 8 and the apparent exchange broadening obtained by the conventional approach, $\Delta R_2(1\ ms^{-1},\infty)$. In accordance with the usual experimental practice, the figure shows the ratio of the exchange contributions at two magnetic field strengths, 11.7 and 14.1 T. The main result is that apparent quadratic scaling, indicated by a ratio of $(14.1/11.7)^2 \approx 1.44$, is obtained for all values of $k_{ex}/\Delta\omega$ provided that $\Delta\omega \leq 1.5/\tau_{cp}$. In practical terms, the apparent field dependence of $R_2(1/\tau_{cp})$ measured for a single value of $1/\tau_{cp}$ under conditions of rapid pulsing ($\tau_{cp} \leq 1$ ms) does not provide any evidence for the time scale of chemical exchange. As shown by eq 16, at least two measurements of $R_2(1/\tau_{cp})$ with τ_{cp} as long and as short as possible are needed at each field to characterize the chemical shift time scale for an exchange process.

The present data comprise an extensive set of relaxation dispersion decays as a function of static field and temperature for BPTI. For the residues with the largest exchange contributions to transverse relaxation, Cys38 and Arg39, dispersion data at both $B_0 = 11.7$ and 14.1 T were fit globally to provide estimates of the exchange parameters, p_a, $\Delta\omega$, and k_{ex}. The fitted values of $\Delta\omega$ for Cys 38 and Arg39 given in Table 4 are in excellent agreement with values of $\Delta\omega = 0.54 \times 10^3\ s^{-1}$ (86 Hz) and $1.15 \times 10^3\ s^{-1}$ (183 Hz), respectively, estimated by Wüthrich and co-workers from zz-exchange spectra recorded at $T = 289$ K and $B_0 = 11.7$ T.[27,49] The values of p_a given in Table 4 also agree with $p_a = 0.96$ estimated by Wüthrich and co-workers. In contrast to earlier reports using data recorded at a single static magnetic field,[14,28] Cys38 and Arg39 exhibit very similar values of $k_{ex} \approx 450\ s^{-1}$ at 300 K and $1340\ s^{-1}$ at 313 K when data from two static magnetic fields is analyzed globally. The activation barrier for the reverse exchange reaction, obtained from the temperature dependence of k_{ex} using the Arrhenius equation, is ~64 kJ/mol. These values agree with apparent activation energies for conformational exchange measured previously in BPTI at lower temperatures using zz-exchange spectroscopy.[27] While the similar exchange rate constants observed for Cys38 and Arg39 support the assumption of a two-state exchange process involving isomerization of the disulfide linkage, k_{ex} or $\Delta\omega$ for Cys14 and Lys15 must be very large, because elevated values of $R_2(1/\tau_{cp})$ were observed at all τ_{cp} values for these residues. This observation suggests that more than one kinetic exchange process may be active in BPTI.[29,50] In general, simultaneous fitting of dispersion data obtained at multiple static magnetic fields will be essential for interpreting exchange phenomena outside of either the slow or fast limits on the chemical shift time scale; however, such analyses can be hindered by small magnitudes of R_{ex}, lack of data over a sufficient range of $1/\tau_{cp}$ values, and violations of the assumption of a two-state exchange process.

Conclusions

Chemical exchange is a ubiquitous phenomenon in NMR spectroscopy that is used for characterizing conformational and kinetic dynamics in molecules ranging from small organic molecules to biological macromolecules. In many cases of practical interest, particularly for macromolecules, the site populations of exchanging chemical species are highly unequal as a consequence of the Boltzmann distribution. Under these conditions, the static magnetic field dependence of the chemical exchange contribution to the transverse relaxation rate constant

(46) Tjandra, N.; Szabo, A.; Bax, A. *J. Am. Chem. Soc.* **1996**, *118*, 6986−6991.
(47) Kroenke, C. D.; Loria, J. P.; Lee, L. K.; Rance, M.; Palmer, A. G. *J. Am. Chem. Soc.* **1998**, *120*, 7905−7915.
(48) Peng, J. W.; Wagner, G. *J. Magn. Reson.* **1992**, *98*, 308−332.
(49) Wider, G.; Neri, D.; Wüthrich, K. *J. Biomol. NMR* **1991**, *1*, 93−98.
(50) Beeser, S. A.; Oas, T. G.; Goldenberg, D. P. *J. Mol. Biol.* **1998**, *284*, 1581−1596.
(51) Shaka, A. J.; Barker, P. B.; Freeman, R. *J. Magn. Reson.* **1985**, *64*, 547−552.
(52) Kay, L. E.; Keifer, P.; Saarinen, T. *J. Am. Chem. Soc.* **1992**, *114*, 10663−10665.
(53) Marion, D.; Ikura, M.; Tschudin, R.; Bax, A. *J. Magn. Reson.* **1989**, *85*, 393−399.

varies as $\delta R_{ex}/R_{ex} = \alpha(\delta B_0/B_0)$, in which $0 \leq \alpha \leq 2$ for $p_a > 0.7$. The value of α depends on the NMR chemical shift time scale for the exchange process. Slow exchange ($k_{ex}/\Delta\omega < 1$) is defined by $0 \leq \alpha < 1$, intermediate exchange ($k_{ex}/\Delta\omega = 1$) is defined by $\alpha = 1$, fast exchange ($k_{ex}/\Delta\omega > 1$) is defined by $1 < \alpha \leq 2$. Therefore, the static magnetic field dependence of R_{ex} determines the chemical shift time scale even if the site populations are so highly skewed that the minor resonance is not observable in the slow exchange limit. The range of values for α observed in basic pancreatic trypsin inhibitor demonstrate that simple assumptions about the field dependence of conformational exchange are frequently erroneous. The scaling factor α is a unique parameter characterizing chemical exchange in NMR spectroscopy and is essential for the interpretation of spin relaxation data acquired at multiple static field strengths.

Acknowledgment. We gratefully acknowledge a discussion with D. A. Torchia (NIH) at the 40th ENC that stimulated our interest in the problem of chemical exchange in systems with skewed site populations. We also acknowledge discussions with M. Rance (University of Cincinnati) that clarified the theoretical results and with L. E. Kay (University of Toronto), concerning the global analysis of dispersion curves. We thank D. A. Torchia and R. Ishima for a preprint of reference 34. O.M. was supported by a predoctoral fellowship awarded by the Ministerio de Educacion y Ciencia (Spain), J.P.L was supported by a National Institutes of Health postdoctoral NRSA (1F32 GM 19247), and C.D.K. was supported by a National Institutes of Health Training Grant (T32 GM08281). M.P. acknowledges a grant from the Direccion General de Enseñanza Superior (PB 97-0933), and A.G.P. acknowledges a grant from the National Institutes of Health (GM 59273).

Supporting Information Available: Four tables containing the measured values of $R_2(1/\tau_{cp})$ at static magnetic field strengths of 11.7 and 14.1 T and temperatures of 300 and 313 K for basic pancreatic trypsin inhibitor (PDF). This material is available free of charge via the Internet at http://pubs.acs.org.

JA993511Y